

Front Motion and Localized States in an Activator-Inhibitor System with Saturation

Arik Yochelis¹ and Alan Garfinkel^{1,2}

¹*Department of Medicine (Cardiology), University of California, Los Angeles, CA 90095*

²*Department of Physiological Science, University of California, Los Angeles, CA 90095*

(Received March 21, 2019)

We study the spatiotemporal dynamics of coherent states (peaks, holes and fronts) in biological systems that exhibit biochemical saturated autocatalysis. Using an activator-inhibitor model equation and a bifurcation analysis, we find the conditions in which two distinct global bifurcation scenarios of coherent states arise. In one of the cases, stable localized hole and peak states are reconnected, and single fronts counter-propagate. These counter-propagating fronts represent a novel mechanism of growth or contraction of activator domains. These phenomena expand the range of biological pattern formation and morphogenesis beyond periodic patterns, and suggest potential therapeutic strategies for patterned pathologies, such as cardiovascular calcification.

PACS numbers: 87.18.Hf, 02.30.Oz, 82.40.Ck, 87.18.La

Reaction-Diffusion (RD) systems display many kinds of pattern formation, ranging from diverse stationary patterns to breathing/replicating spots and spiral waves [1]. One important application of RD systems is to biological pattern formation and morphogenesis, as originally suggested by Turing: reaction and diffusion of two chemical substances ('morphogens'), at different rates, can induce spontaneous symmetry-breaking of a homogeneous state and thus form patterns [2]. Turing described a simple activator-inhibitor system; since then, many model equations in physical, chemical and biological contexts have been shown to form periodic patterns via a Turing-type instability [1, 3, 4]. There is a significant difference between chemical systems and biological media: In the latter, the formation of labyrinthine patterns, for example, has been attributed to the phenomenon of *saturation* [5].

Coherent states are another important property of RD media; we distinguish between *heteroclinic* orbits (fronts) and *homoclinic* orbits (localized states) in one-dimensional (1D) physical space. In the past, the formation of localized states in bistable systems was often linked to interactions between two front solutions [6]. However, this approach requires a large separation between two interacting fronts and thus is not valid for the analysis of spatial homoclinic orbits. By a different method, it was recently shown that localized states in variational systems are intimately related to Maxwell points, and thus nonpropagating fronts, connecting either two uniform states [7] or a uniform and a periodic [8] state. In the second case, there can be an effective broadening of the Maxwell point so that stationary fronts exist over a finite parameter range [9]; this phenomenon is referred to as *pinning*. While biological patterns have been extensively studied in the context of periodic patterns [3], there is no unified theory of coherent states (localized and fronts) and the resulting spatiotemporal dynamics in systems that involve autocatalytic saturation.

Here we study the formation mechanisms of localized states and front motion in a bistable activator-inhibitor system with saturated autocatalysis. Surpris-

ingly, we find two types of bounded and unbounded localized states; these are localized 'hole' and 'peak' states. In the first case, we explain why only hole solutions exhibit bounded behavior which is similar to the *continuous branch pinning* (CBP) seen in variational systems [8]. In this limit, the finite amplitude activator state always invades a trivial state, producing activator expansion. On the contrary, in the second case, a single activator front can also counter-propagate, producing activator contraction. The mechanism is different from the unfolded non-equilibrium Ising-Bloch bifurcation [10]. In this regime, the stable hole and peak branches are reconnected; the hole branches form a novel pinning class, *discontinuous branch pinning* (DBP). As a consequence, front counter-propagation and the existence of localized states give rise to an activator domain growth or contraction and a simultaneous formation of embedded localized axisymmetric or striped states, as shown in Fig. 1.

We start with a phenomenological activator-inhibitor model introduced by Gierer and Meinhardt [11], to study biological pattern formation. Our interest in this model stems from calcification in vascular-derived mesenchymal stem cell (VMSC) cultures [12], cells that considered to be responsible for cardiovascular calcification [13]. Particularly, it is biochemically assumed that the activator obeys a saturated autocatalytic reaction [14] and promotes production of the inhibitor [15]. The cells also express a rapidly diffusing inhibitor [12]. This biochemical activator-inhibitor dynamics therefore qualitatively rationalize the framework of Gierer-Meinhardt model [5, 11], which in its dimensionless form reads

$$\begin{aligned}\frac{\partial u}{\partial t} &= D\nabla^2 u + \frac{u^2 v^{-1}}{1 + u^2} - u, \\ \frac{\partial v}{\partial t} &= \nabla^2 v + Pu^2 - Ev + S,\end{aligned}\tag{1}$$

where $u(x, y)$ is activator, $v(x, y)$ is inhibitor, D is the diffusion ratio, P augments the cross reaction rates, E is the degradation ratio and S is the generalized inhibitor source term. Due to the interest in vascular calcification [13], we chose here the parameters estimated in [12]

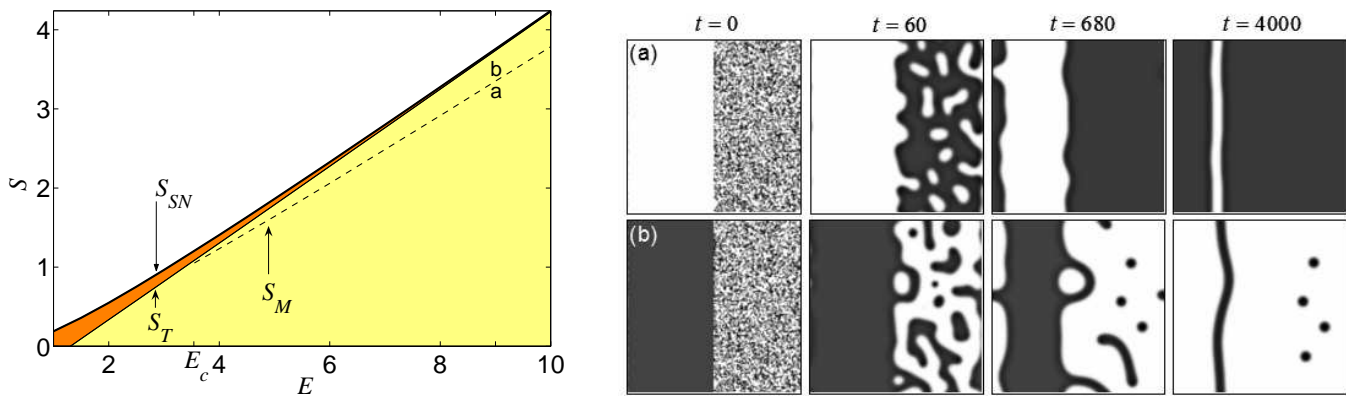


FIG. 1: (color online) Left panel: Bistability region, $S < S_N$, of uniform solutions $(0, v_0)$ and (u_+, v_+) in the $E - S$ plane (shaded region). The dark shaded region, $S_T < S < S_{SN}$, marks the linear instability of the uniform (u_+, v_+) state to nonuniform perturbations, where S_T is the onset of Turing instability. The dashed line $S = S_M$, for $E > E_c \simeq 3.54$, represents the stationary front between $(0, v_0)$ and (u_+, v_+) states. For $S < S_M$, (u_+, v_+) invades $(0, v_0)$ while for $S_M < S < S_T$ $(0, v_0)$ invades (u_+, v_+) . Right panel: Demonstration of the activator (a) expansion and (b) contraction process at marked locations in the left panel, stationary front $S = S_M \simeq 3.35$ for $E = 9$, via numerical integration of Eq. (1) on $x = y = [0, 15]$ domain with periodic boundary conditions. The frames show a grey-scale map of the u field, where black denotes a high value of u . The initial condition is either uniform (a) $u = 0.01$ or (b) $u = 1$ in the left half of the domain, while the right half is a uniform random distribution between 0.01 and 1. Parameters: (a) $S = 3.3$, (b) $S = 3.4$, and for both $P = 1$, $D = 0.005$.

(see supporting online supplement), i.e., $P \sim \mathcal{O}(1)$, $D \sim \mathcal{O}(10^{-2} - 10^{-3})$, and focus on the two remaining parameters S and E , which are experimentally accessible. We note that localized peaks have also been studied in other forms of (1), in 1D and 2D [16].

Eq. (1) admits three uniform solutions, one of which $(u, v) = (0, v_0) \equiv (0, S/E)$ is trivial, and two non trivial $(u, v) = (u_{\pm}, v_{\pm})$. For $P = 1$ considered here, the nontrivial solutions are given by $[u_{\pm}, v_{\pm}] = [(\sqrt{\theta} \pm \sqrt{\eta})/2, \sqrt{\theta}(\sqrt{\theta} \pm \sqrt{\eta})/(E - (S - 1)\sqrt{\theta} \pm \theta\sqrt{\eta})]$, where $\eta \equiv 2E/\sqrt{\theta} + \phi$, $\theta \equiv \beta/3\rho + \rho/3 - 2(S + 1)/3$, $\phi \equiv -\theta - 2(S + 1)$, $\rho \equiv (\alpha/2 + \sqrt{\alpha^2/4 - \beta^3})^{1/3}$, $\alpha \equiv 27E^2 - 72S(S + 1) + 2(S + 1)^3$, $\beta \equiv 1 + 14S + S^2$. Uniform (u_-, v_-) states appear as unstable states from $S = 0$ and annihilate with the stable (u_+, v_+) branch at a saddle-node bifurcation, $S = S_{SN}$, creating bistability between $(0, v_0)$ and (u_+, v_+) for $0 < S < S_{SN}$. A primary requirement for both localized and front solutions is the linear stability of the uniform solutions to nonuniform perturbation. Standard linear analysis of $(0, v_0)$ and (u_+, v_+) yields that only the nontrivial state goes through a Turing instability at $S = S_T$. The unstable Turing region $S_T < S < S_{SN}$ shrinks by approaching the saddle node bifurcation, $S = S_{SN}$, as the degradation ratio E is increased (see Fig. 1). Consequently, stable front solutions connecting the uniform (u_+, v_+) and $(0, v_0)$ states exist below $S = S_T$.

We study the properties of localized states via *spatial dynamics* [17] followed by numerical branch continuation method [18] and temporal eigenvalue analysis. We set $\partial_t u = \partial_t v = 0$ and analyze (1) as a reversible ordinary differential equation due to the $x \rightarrow -x$ invariance. Linearizations about the uniform states result in steady state solutions which are proportional to $\exp(\lambda x)$, where

the spatial eigenvalue λ satisfies a fourth order algebraic equation. For the (u_+, v_+) case, three possible solutions for λ in complex phase space arise: (i) for $S > S_T$ the eigenvalues split on the imaginary axis; (ii) for $S < S_T$ they split and form a complex quartet; and (iii) at the Turing onset, $S = S_T$, a double multiplicity of pure imaginary eigenvalues $\lambda = \pm ik_T$ is present, where k_T is the critical Turing mode. We note that the domain size used in our numerical calculations is much larger than the spatial period $2\pi/k_T$. Thus, localized states that exponentially asymptote to (u_+, v_+) can be expected to arise for $S < S_T$. On the other hand, linearization about $(0, v_0)$ yields four real eigenvalues, $\lambda = \pm\sqrt{E}$ and $\lambda = \pm\sqrt{D^{-1}}$. Thus, localized states that exponentially asymptote to $(0, v_0)$ are expected to arise everywhere. For finite values of E , bifurcation of these states is at the transcritical onset, $S = 0$ (the mechanism will be discussed elsewhere). In the following, we refer to L^+ as ‘holes’ while to L^0 as ‘peaks’ in the background of the nontrivial and trivial activator fields, respectively.

To study the localized solutions *far* from the onset, we implement a numerical branch continuation method [18]; the results are presented as a function of S in terms of the norm

$$N = \sqrt{\frac{1}{L} \int_0^L [u^2 + v^2 + (\partial_x u)^2 + (\partial_x v)^2] dx}, \quad (2)$$

where L is the spatial period. We distinguish between two qualitatively distinct regions (see Fig. 1): $E < E_c$, where the holes and peaks do not overlap, and $E > E_c$ (see Fig. 2), where peaks and holes merge at $S = S_M$, and formation of a stationary front between (u_+, v_+) and $(0, v_0)$ (see Fig. 3).

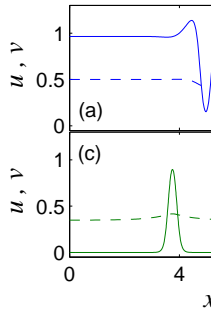
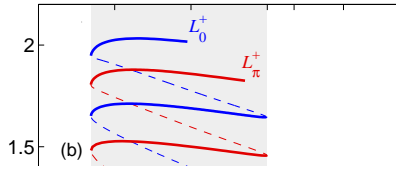


FIG. 2: (color online) Bifurcation diagram for Eq. (1) in 1D, showing branches of localized states. The shaded region marks the stable portion of the branches. S_T and S_{SN} denote the onset of Turing instability (solid line) and the onset of saddle-node bifurcation (dashed line). The stable portions of the branches are determined by time integration of Eq. (1) for $S \simeq 0.696$, (d) $S \simeq 1.233$, $P = 1$.

First, we discuss the $E < E_c$ case. Localized hole solutions, L^+ , bifurcate as unstable small amplitude states, from the Turing onset, $S = S_T$, and form a CBP region via a *homoclinic snaking* (shaded region in Fig. 2), as also happens in variational systems [8]. Since the localized holes bifurcate from a nontrivial state, only two even parity solutions with phase shifts of π can form. Thus, we termed a branch with an odd number of holes as L_0^+ [Fig. 2(a)] and the one with an even number as L_π^+ [Fig. 2(b)]. Here we used a relatively small domain which limits further excursions of the two branches (Fig. 2), while on an infinite domain, the branches contain an infinite number of saddle node points. On the other hand, the localized states that are homoclinic to the $(0, v_0)$ state bifurcate from $S = 0$ and do not form a pinning region, due to real eigenvalues. These states contain only a single stable branch of L_0^0 while the other even branch L_π^0 is unstable [see profiles (c,d) in Fig. 2], denoting a repulsive

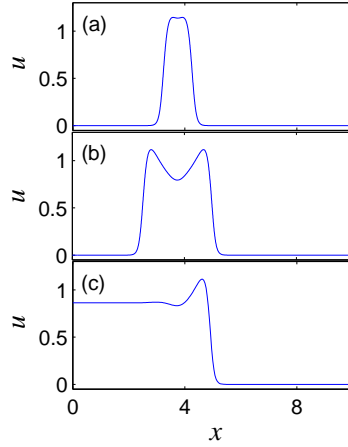
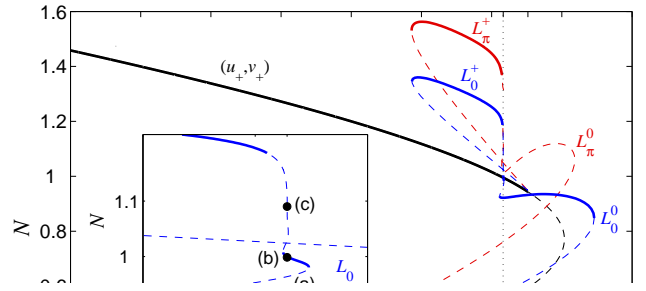


FIG. 3: (color online) Top Panel: Bifurcation diagram for $E = 4$. The inset in the top panel clarifies the behavior of L_0^+ and L_0^0 branches at $S = S_M \simeq 1.233$. Bottom panels: Profiles of u at locations indicated in the inset. Other parameters as in Fig. 2.

interaction between two neighboring peaks.

Next, we turn to discussion of the second case, $E > E_c$. We showed in Fig. 1, that increase in E results in $S_T \rightarrow S_{SN}$. Above $E = E_c \simeq 3.54$, this shift causes an overlapping between the CBP region of hole states and the peak states that are present near the saddle node $S = S_{SN}$. This hole-peak interaction allows formation of a time independent heteroclinic orbit at $S = S_M$, connecting the trivial and the nontrivial states. All the localized state branches that were present in the $E < E_c$ case, now collapse nonmonotonically at $S = S_M$. The single and the double hole state, $L = L^+$, still bifurcate from the Turing onset (see Fig. 3), but all other branches (not shown here for simplicity) arise from and reconnect after a single excursion, back to $S = S_M$. This DBP structure is fundamentally different from the classical CBP, described for $E < E_c$ and in [8]. The L^0 branches also go through a significant change: while L_π^0 remains unstable, the L_0^0 branch exhibits decreasing oscillations around $S = S_M$ (see inset of Fig. 3). This behavior is known to give rise to additional localized states [7, 19], with weak spatial oscillations around the primary peak [see Fig. 3(b)].

The activator expansion or contraction and formation of isolated stripes and axisymmetric localized states (Fig. 1) is now transparent. The merging point, $S = S_M$, separates regions of counter-propagating single fronts.

Thus, opposite front velocities and the simultaneous presence of stable localized holes, peaks and stripes, result in a nontrivial behavior for bistable non-variational systems with a broken parity symmetry. In the absence of localized states, the system converges to a finite uniform activator state, a phenomenon that is qualitatively similar to coarsening in variational systems [6]. An additional important aspect is the stability of coherent structures to curvature and transverse perturbations in 2D. While stability thresholds of localized states may indeed change in 2D, the 1D analysis delimits the regions where stable localized states can also be obtained in 2D, as shown in Fig. 1. By contrast, instability to transverse perturbations of the front solutions or large circular domains may lead to the formation of periodic patterns that resemble periodic patterns arising from the Turing instability [20]. In our parameter range these fronts are stable, but we cannot exclude the existence of transverse instabilities in general.

We have demonstrated a novel mechanism of activator

expansion or contraction and the respective formation of localized states in an asymmetric bistable activator-inhibitor system with saturated autocatalysis, as shown in Fig. 1. This mechanism stems from the merging of all coherent states at a single point in parameter space, and not from the non-equilibrium Ising-Bloch bifurcation [6, 10]. In addition, we uncovered a new discontinuous branch pinning structure, which gives rise to bounded localized states, as shown in Fig. 3. Furthermore, our theoretical results suggest a distinct spatiotemporal behavior in biological systems exhibiting saturation [5]. The concept of activator contraction is potential biomedical applications, for example, localized activator-induced ‘nodules’ are common in biomedicine, such as spotty formations in atherosclerotic calcification [21]. The ability to produce conditions of ‘activator contraction’ to reduce or eliminate these localized spots has intriguing therapeutic potential.

We thank L.L. Demer, Y. Tintut, K. Boström, E. Knobloch and J. Burke for stimulating discussions.

-
- [1] M.C. Cross and P.C. Hohenberg, *Rev. Mod. Phys.* **65**, 851 (1993); P.K. Maini, K.J. Painter, and H.N.P. Chau, *J. Chem. Soc., Faraday Trans.* **93**, 3601 (1997); P.K. Maini, *C. R. Biologies* **327**, 225 (2004).
- [2] A. Turing, *Philos. Trans. R. Soc. London, Ser. B* **237**, 37 (1952).
- [3] S. Kondo and R. Asai, *Nature (London)* **376**, 765 (1995); K.J. Painter, P.K. Maini, and H.G. Othmer, *Proc. Natl. Acad. Sci.* **96**, 5549 (1999); M.P. Harris *et al.*, *Proc. Natl. Acad. Sci.* **102**, 11734 (2005); S. Sick, S. Reinker, J. Timmer, T. Schlake, *Science* **314**, 1447 (2006); M. Yamaguchi, E. Yoshimoto, and S. Kondo, *Proc. Natl. Acad. Sci.* **104**, 4790 (2007); J.D. Murray, *Mathematical Biology* (Springer, New York, 2002).
- [4] J. von Hardenberg, E. Meron, M. Shachak, and Y. Zarmi, *Phys. Rev. Lett.* **87**, 198101 (2001); Y.-J. Li *et al.*, *Science* **291**, 2395 (2001); J.H.E. Cartwright, *J. Theor. Biol.* **217**, 97 (2002); A. Yochelis *et al.*, *SIAM J. Appl. Dyn. Syst.* **1**, 236 (2002).
- [5] A.J. Koch and H. Meinhardt, *Rev. Mod. Phys.* **66**, 1481 (1994).
- [6] P. Coulet, *Int. J. Bifurcation Chaos* **12**, 2445 (2002); L.M. Pismen, *Patterns and Interfaces in Dissipative Dynamics* (Springer-Verlag, Berlin Heidelberg, 2006).
- [7] J. Knobloch and T. Wagenknecht, *Physica (Amsterdam)* **206D**, 82 (2005).
- [8] P.D. Woods and A.R. Champneys, *Physica (Amsterdam)* **129D**, 147 (1999); P. Coulet, C. Riera, and C. Tresser, *Phys. Rev. Lett.* **84**, 3069 (2000); J. Burke and E. Knobloch, *Phys. Rev. E* **73**, 56211 (2006).
- [9] Y. Pomeau, *Physica (Amsterdam)* **23D**, 3 (1986).
- [10] A. Hagberg and E. Meron, *Chaos* **4**, 477 (1994).
- [11] A. Gierer and H. Meinhardt, *Kybernetik* **12**, 30 (1972).
- [12] A. Garfinkel *et al.*, *Proc. Natl. Acad. Sci.* **101**, 9247 (2004).
- [13] Y. Tintut *et al.*, *Circulation* **108**, 2505 (2003); M. Abedin, Y. Tintut, and L.L. Demer, *Circ. Res.* **95**, 671 (2004); K.A. Hruska, S. Mathew, and G. Saab, *Circ. Res.* **97**, 105 (2005). J.-S. Shao, J. Cai, and D.A. Towler, *Arterioscler. Thromb. Vasc. Biol.* **26**, 1423 (2006).
- [14] N. Ghosh-Choudhury *et al.*, *Biochem. Biophys. Res. Commun.* **286**, 101 (2001).
- [15] A. F. Zebboudj, V. Shin and K. Boström, *J. Cell Biochem.* **90**, 756 (2003).
- [16] A. Doelman and H. van der Ploeg, *SIAM J. Appl. Math.* **1**, 65 (2002); M. Ward *et al.*, *SIAM J. Appl. Math.* **62**, 1297 (2002); T. Kolokolnikov, W. Sun, M. Ward, and J. Wei, *SIAM J. Appl. Dyn. Syst.* **5**, 313 (2006).
- [17] A.R. Champneys, *Physica (Amsterdam)* **112D**, 158 (1998).
- [18] E. Doedel *et al.*, “*AUTO2000: Continuation and bifurcation software for ordinary differential equations*,” Technical report, Concordia University (2002).
- [19] A. Yochelis, J. Burke, and E. Knobloch, *Phys. Rev. Lett.* **97**, 254501 (2006).
- [20] A. Hagberg, E. Meron, *Chaos* **4**, 477 (1994); R.E. Goldstein, D.J. Muraki, and D.M. Petrich, *Phys. Rev. E* **53**, 3933 (1996); A. Yochelis, C. Elphick, A. Hagberg, and E. Meron, *Physica (Amsterdam)* **199D**, 201 (2004); D. Gomila, P. Colet, G.-L. Oppo, and M. San Miguel, *J. Opt. B: Quantum Semiclass. Opt.* **6**, S265 (2004); T. Kolokolnikov and M. Tlidi, *Phys. Rev. Lett* **98**, 188303 (2007).
- [21] M. Abedin, Y. Tintut, and L.L. Demer, *Arterioscler. Thromb. Vasc. Biol.* **24**, 1161 (2004).